expansion (Fig. 3) (*3, 9, 10, 12, 29–31*). Because the temperature of the inner core is believed to be close to the melting curve of Fe, the extrapolated V_S of hcp-Fe in the inner core should be corrected to even lower values. The small deviation in V_P between shock-wave data (*3*) and the previous NRIXS study (*10*) at high pressures and room temperature also suggests that the temperature effect on V_P is suppressed under inner core conditions, whereas the large difference in the V_S indicates that temperature has a strong effect on V_S even under core pressures (Fig. 3). Theoretical calculations on the elasticity of hcp-Fe predicted that V_S and G would decrease with increasing temperature at a constant density of 13.04 g cm^{-3} (*11*).

Birch pointed out the likely temperature effect on the sound velocities in his original paper in 1961 (*2*). Our results confirm this idea. It has been shown that the addition of a light element such as Si or S into Fe increases V_P and V_S under high pressures (*32, 33*). Considering the temperature effect on V_P and V_S of hcp-Fe at inner core pressures and 6000 K (*20*), a few percent of light elements alloyed with Fe are still needed in the inner core to increase V_P to match seismic models (Fig. 3). This results in more light elements in Earth's inner core than has been suggested from the linearly extrapolated V_P of hcp-Fe at high pressures and room temperature (*12*).

References and Notes

1. F. Birch, *J. Geophys. Res.* **57**, 227 (1952).
2. F. Birch, *Geophys. J. R. Astron. Soc.* **4**, 295 (1961).
3. J. M. Brown, R. G. McQueen, *J. Geophys. Res.* **91**, 7485 (1986).
4. J. D. Bass, B. Svendsen, T. J. Ahrens, in *High Pressure Research in Mineral Physics*, M. H. Manghnani, Y. Syono, Eds. (American Geophysical Union, Washington, DC, 1987), pp. 393–423.
5. H. K. Mao, Y. Wu, L. C. Chen, J. F. Shu, *J. Geophys. Res.* **95**, 21737 (1990).
6. H. K. Mao et al., *Nature* **396**, 741 (1999).
7. G. Steinle-Neumnn, L. Stixrude, R. E. Cohen, *Phys. Rev. B* **60**, 791 (1999).
8. D. Alfe, M. J. Gillan, G. D. Price, *Nature* **405**, 172 11 (2000).
9. G. Fiquet, J. Badro, F. Guyot, H. Requardt, M. Krisch, *Science* **291**, 468 (2001).
10. H. K. Mao et al., *Science* **292**, 914 (2001).
11. G. Steinle-Neumann, L. Stixrude, R. E. Cohen, *Nature* **413**, 57 (2001).
12. D. Antonangeli et al., *Earth Planet. Sci. Lett.* **225**, 243 (2004).
13. J. H. Nguyen, N. C. Holmes, *Nature* **306**, 2239 (2004).
14. R. C. Liebermann, A. E. Ringwood, *J. Geophys. Res.* **78**, 6926 (1973).
15. A. J. Campbell, D. L. Heinz, *Science* **257**, 66 (1992).
16. W. Sturhahn et al., *Phys. Rev. Lett.* **74**, 3832 (1995).
17. W. Sturhahn, V. G. Kohn, *Hyperfine Interactions* **123/124**, 367 (1999).
18. M. Hu et al., *Phys. Rev. B* **67**, 094304 (2003).
19. R. Lübbers, H. F. Grünsteudel, A. I. Chumakov, G. Wortmann, *Science* **287**, 1250 (2000).
20. Materials and methods are available as supporting material on *Science* Online.
21. J. F. Lin et al., *Geophys. Res. Lett.* **31**, L14611 (2004).
22. G. Shen et al., *Phys. Chem. Miner.* **31**, 353 (2004).
23. L. S. Dubrovinsky, S. K. Saxena, P. Lazor, *Phys. Chem. Miner.* **25**, 434 (1998).
24. L. S. Dubrovinsky, S. K. Saxena, F. Tutti, S. Rekhi, *Phys. Rev. Lett.* **84**, 1720 (2000).
25. L. S. Dubrovinsky, S. K. Saxena, N. A. Dubrovinskais, S. Rekhi, T. LeBihan, *Am. Mineral.* **85**, 386 (2000).
26. F. Birch, *J. Geophys. Res.* **83**, 1257 (1978).
27. W. Mao et al., *Geophys. Res. Lett.* **31**, L15618 (2004).
28. D. L. Heinz, *Geophys. Res. Lett.* **17**, 1161 (1990).
29. A. M. Dziewonski, D. L. Anderson, *Phys. Earth Planet. Inter.* **25**, 297 (1981).
30. L. S. Dubrovinsky, N. A. Dubrovinskais, T. LeBihan, *Proc. Natl. Acad. Sci. U.S.A.* **98**, 9484 (2001).
31. O. L. Anderson, L. S. Dubrovinsky, S. K. Saxena, T. LeBihan, *Geophys. Res. Lett.* **28**, 399 (2001).
32. J. F. Lin et al., *Geophys. Res. Lett.* **28**, 2112 (2003).
33. J. F. Lin et al., *Earth Planet. Sci. Lett.* **226**, 33 (2004).
34. This work and use of the APS are supported by the U.S. Department of Energy (DOE), Basic Energy Sciences (BES), Office of Science, under contract no. W-31-109-ENG-38, and by the state of Illinois under the Higher Education Cooperation Act. We thank GeoSoilEnviroCARS and APS for the use of the ruby fluorescence system and E. E. Alp, D. Errandonea, S.-K. Lee, V. Struzhkin, M. Hu, D. L. Heinz, G. Steinle-Neumann, R. Cohen, J. Burke, V. Prakapenka, M. Rivers, S. Hardy, T. Duffy, and J. M. Jackson for their help and discussions. Work at Carnegie was supported by DOE/BES, DOE/National Nuclear Security Administration (Carnegie/DOE Alliance Center), NSF, and the W. M. Keck Foundation.

Deep-Sea Temperature and Circulation Changes at the Paleocene-Eocene Thermal Maximum

Aradhna Tripati* and Henry Elderfield

A rapid increase in greenhouse gas levels is thought to have fueled global warming at the Paleocene-Eocene Thermal Maximum (PETM). Foraminiferal magnesium/calcium ratios indicate that bottom waters warmed by 4° to 5°C, similar to tropical and subtropical surface ocean waters, implying no amplification of warming in high-latitude regions of deep-water formation under ice-free conditions. Intermediate waters warmed before the carbon isotope excursion, in association with downwelling in the North Pacific and reduced Southern Ocean convection, supporting changing circulation as the trigger for methane hydrate release. A switch to deep convection in the North Pacific at the PETM onset could have amplified and sustained warming.

PETM was a short-lived global warming event about 55 million years ago (Ma) that may provide insights into the environmental consequences of rising greenhouse gas levels (*1, 2*). A reduction in the carbonate content of deep-sea sediments (*2*) and a large negative excursion in marine and terrestrial carbon isotope (δ^{13}C) records (*1–3*) are associated with the PETM and indicate the addition of ^{13}C-depleted carbon to the oceans and atmosphere. A possible source of this carbon was the dissociation of ~1000 to 2100 gigatons (Gt) of methane hydrate in ocean sediments (*4*), most or all of which would have oxidized, raising atmospheric CO_2 by 70 to 160 parts per million by volume (ppmv) (*5, 6*). Benthic foraminiferal taxa exhibit increased extinction rates during the PETM, probably because of deep-sea oxygen deficiency and a decrease in seawater carbonate ion concentration (*2*).

The climatic response to rising greenhouse gas levels in the past has been debated because of equivocal ocean temperature reconstructions based on foraminiferal oxygen isotope ratios ($\delta^{18}O_C$), which are a function of both temperature and seawater δ^{18}O ($\delta^{18}O_W$). To circumvent this ambiguity, the Mg/Ca temperature proxy has been applied to planktonic foraminifera, and it documented a 4 to 5°C warming of sea-surface temperatures (SST) across the PETM in the subtropical (*7*) and tropical ocean (*7, 8*).

We investigated the evolution of deep-sea temperatures, high-latitude SST, and circulation patterns using foraminiferal Mg/Ca and stable isotope ratios (*9, 10*) in order to examine the causes and consequences of the δ^{13}C excursion and the PETM. We used Mg/Ca ratios of benthic foraminifera to develop estimates of bottom water temperatures (T_B) for deep sites in the subtropical South Atlantic (Site 527) and tropical North Pacific (Site 1209) oceans, and for a site at intermediate depths in the equatorial Pacific Ocean (Site 865) (table S1). These temperatures should reflect surface conditions in high-latitude regions of deep-water formation. We integrated these data with SST records (*7, 8*) to study the spatial pattern of warming and changes in the

Department of Earth Sciences, University of Cambridge, Downing Street, CB2 3EQ, UK.

*To whom correspondence should be addressed. E-mail: atri02@esc.cam.ac.uk

thermal structure of the tropical oceans. We also constructed the first benthic stable isotope record for the deep Pacific through the PETM for comparison with published records from South Atlantic Sites 527 (2) and 690 (Atlantic sector, Southern Ocean) (1), in order to investigate basinal gradients in T_B, $\delta^{18}O_W$ and $\delta^{13}C$.

Late Paleocene T_B (Fig. 1) at Atlantic Site 527 were 12 to 13°C (~3400 m in paleodepth), similar to previous early Cenozoic estimates (11). Pacific temperatures were warmer, with T_B at deep Site 1209 of ~14°C (~2400 m in paleodepth), and >16°C at intermediate Site 865 (~1300 m in paleodepth). The record of T_B for Pacific Site 865 indicates 2 to 3°C warming at intermediate depths between 55.60 and 55.50 Ma, before the $\delta^{13}C$ excursion. Coincident with the $\delta^{13}C$ excursion is an abrupt increase in benthic foraminiferal Mg/Ca ratios, indicating warming of 3°C at the intermediate site and of 4°C at the two deep sites. Estimated peak T_B are 21°C and 17°C, respectively, similar to recent estimates based on dinoflagellates (12) of Arctic Ocean surface temperatures for the PETM. At all sites, T_B decreased within 50,000 years after the $\delta^{13}C$ excursion and reached Late Paleocene background values after 150,000 to 200,000 years, ~50,000 years after $\delta^{13}C$ values recover.

Basinal $\delta^{13}C$ gradients (13–15) and modeling (16) show deep waters would have formed in the high latitudes during the late Paleocene and early Eocene. Tropical and subtropical SST from Mg/Ca ratios show warming of 4 to 5°C (7, 8), implying that the zonal pattern of surface ocean warming was relatively uniform during the PETM. This paleoclimatic response is consistent with minimal sea ice and continental ice during the Late Paleocene, as melting would have accelerated high-latitude warming through ice-albedo feedbacks. The pole-to-equator temperature gradient (presuming convection occurred in the high latitudes) shows no discernable change associated with the carbon release, with a gradient of 19.0 ± 1°C before the carbon isotope excursion and 19.5 ± 1°C during the PETM. Thus, in the absence of extensive continental ice sheets and sea ice, rising greenhouse gas levels resulted in ocean warming at all latitudes, with no detectable amplification of warming in the high-latitude regions of deep-water formation.

$\delta^{18}O_W$ covaries with salinity and is estimated by subtracting the temperature component from benthic $\delta^{18}O_C$ (Fig. 2A) (1). From the late Paleocene to the PETM peak, the calculated $\delta^{18}O_W$ decrease at South Atlantic Site 527 is 0.1 to 0.3 per mil (‰), indicating that deep waters freshened in association with warming. At Southern Ocean Site 690, the $\delta^{18}O_W$ decrease is 0.4 to 0.6‰, giving a larger amount of freshening. Global warming is thought to have

enhanced precipitation in the high latitudes of the Southern Hemisphere because of greater vapor transport from the subtropics (16), and there is also evidence for higher subtropical surface water salinities at the PETM (7). In contrast, at Site 1209, $\delta^{18}O_W$ increased by 0.3 to 0.5‰, indicative of more saline deep waters in the North Pacific during the PETM.

Hydrographic sections (Fig. 3) derived by combining estimates of T_B for different depths

with mixed-layer and thermocline temperatures for the tropical Pacific (fig. S1) show that the entire water column warmed by 4 to 5°C and that the earliest Eocene thermal structure was similar to that of the Latest Paleocene. Combining this with $\delta^{18}O_C$ indicates that the tropical Pacific vertical salinity gradient must have evolved substantially, with an increase in deep-water salinity and a freshening of overlying waters during the PETM reflect-
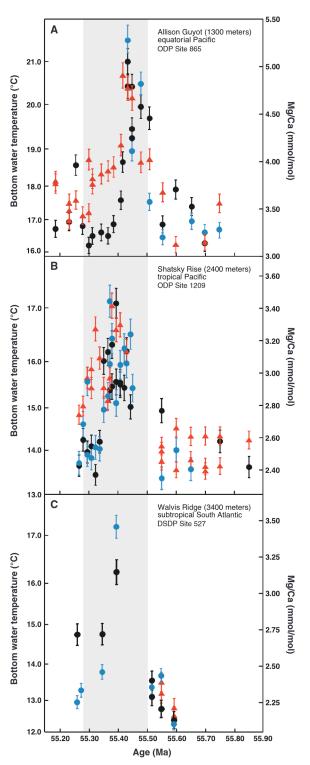

Fig. 1. High-resolution benthic foraminiferal Mg/Ca records across the PETM and corresponding temperature scale (black circles, *Oridorsalis umbonatus*; blue circles, *Nuttallides truempyi*; red triangles, *Cibicidoides* spp.). (**A**) Allison Guyot, ODP site 865 (equatorial Pacific Ocean, 1300 m in depth). (**B**) Shatsky Rise, ODP site 1209 (tropical North Pacific Ocean, 2400 m in depth). (**C**) Walvis Ridge, Deep-Sea Drilling Program (DSDP) site 527 (subtropical South Atlantic Ocean, 3400 m in depth). Mg/Ca ratios are normalized to *O. umbonatus* (30). The PETM interval (55.50 to 55.28 Ma) is highlighted (gray bar). In order to place results on a common age scale, we used reported datum levels for the carbon isotope base, peak, and recovery and also used the reported first occurrence of *Discoaster multiradiatus* and *Fasculithes tympaniform* (table S3). Planktic foraminiferal $\delta^{13}C$ data are shown in fig. S3. Absolute chronologies for the PETM are subject to revision.

ing a sensitive hydrologic cycle and/or changing ocean circulation.

The Latest Paleocene intermediate water warming would likely have destabilized large regions of sedimentary methane hydrates, added ^{13}C-depleted carbon to the oceans and the atmosphere, and initiated the PETM (*4, 16*). To assess whether changing ocean circulation could have triggered intermediate water warming, we inferred deep-water source regions by constraining aging, temperature, and salinity gradients between the South Atlantic, Southern Ocean, and North Pacific during four time intervals. As waters sink and flow through the ocean, they accumulate respired ^{12}C-rich CO_2 and nutrients from the remineralization of raining organic matter, so that young, recently ventilated, deep waters will have higher δ^{13}C than deep waters that are further from source regions.

1) Late Paleocene (>55.60 Ma): Benthic δ^{13}C values for Pacific Site 1209 are ~0.5‰ lower than at the Atlantic (Figs. 2B and 4) and Southern Ocean sites (fig. S2), implying that South Atlantic waters were ventilated more recently than those in the North Pacific. Differences in surface water productivity between regions can also affect δ^{13}C gradients between sites, and the Southern Ocean site may have experienced relatively large changes in productivity across the PETM (*17*). However, the other sites would have been located within subtropical gyres (*16*), characterized by relatively low-productivity surface waters. Comparison of $\delta^{18}O_C$ and T_B shows that bottom waters at the Pacific site were ~1°C warmer and similar in salinity to bottom waters at the Atlantic and Southern Ocean sites (Fig. 4 and fig. S2) and therefore were less dense. Thus, the data are consistent with deep ocean overturning being driven by convection in the Southern Ocean (*13–15, 18*).

2) Latest Paleocene (55.60 to 55.50 Ma): The δ^{13}C differences between the three sites decrease, converging by the onset of the δ^{13}C excursion, suggesting that deep water was aging in the South Atlantic and becoming younger in the North Pacific. Waters at the Pacific site became more saline, whereas at the Atlantic site they became slightly fresher and warmer by 1°C (Fig. 4 and table S2). The decrease in planktonic foraminiferal $\delta^{18}O_C$ at Site 690 (*19*) indicates Southern Ocean surface waters also became fresher and/or warmer. These findings suggest that deep-water formation in the Southern Ocean decreased with the gradual development of a second circulation cell in the North Pacific, coincident with intermediate water warming in the Pacific.

3) PETM (~55.45 Ma): Samples from the peak of the PETM indicate a distribution in deep-water δ^{13}C very different from previous distributions. Although the whole-ocean shift in δ^{13}C records the injection of ^{13}C-depleted

carbon, the differences in δ^{13}C imply that bottom waters at the Pacific site were younger than at the Atlantic and Southern

Ocean sites. Deep waters would have been ^{13}C-poor because of weak rates of overturning in the Southern Ocean and slow
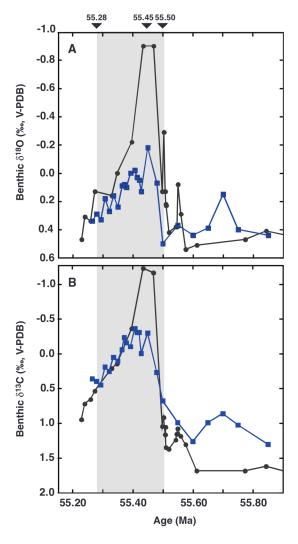

Fig. 2. (**A**) Benthic foraminiferal δ^{18}O for deep sites in the North Pacific (blue line, ODP Site 1209, Shatsky Rise) and South Atlantic (dark gray line, DSDP Site 527, Walvis Ridge). Black triangles point to datum levels. Not shown are two additional datum levels (56.20 and 55.00 Ma) that were used to constrain the age models for both sites. The PETM interval is shaded. (**B**) Benthic foraminiferal δ^{13}C for deep sites in the North Pacific and South Atlantic. V-PDB, Vienna Peedee Belemnite.
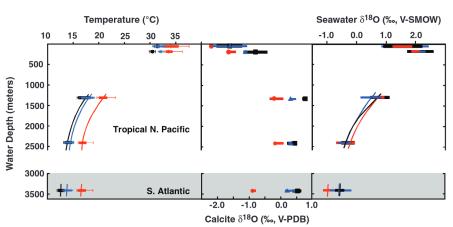

Fig. 3. Vertical profiles of temperature, foraminiferal δ^{18}O, and seawater δ^{18}O for the tropical Pacific for different time slices during the Late Paleocene (black), PETM (red), and Earliest Eocene (blue). Mixed-layer temperatures and thermocline temperatures are estimated with planktonic foraminiferal Mg/Ca values at ODP Sites 1209 and 865 (fig. S1) (*7, 8*) and with benthic foraminiferal Mg/Ca–based T_B for sites at different water depths (Fig. 1). Means (symbols), the range of estimates (thick lines), and error bars (thin lines) are shown for each interval. Data for the South Atlantic (DSDP Site 527) are shown in the shaded panel for comparison. V-SMOW, Vienna Standard Mean Ocean Water.

ventilation rates in South Atlantic basins. Elevated Southern Ocean productivity accompanying the PETM (*17*) may have also enhanced the $\delta^{13}C$ contrast with the deep Pacific. Bottom waters at the Pacific site were similar in temperature to those of the Atlantic and Southern Ocean sites, but more salty. These results indicate that the PETM was associated with a unique mode of ocean circulation, with a saline and warm North Pacific deep-water mass that was younger and more dense than South Atlantic and Southern Ocean waters, consistent with convection in the North Pacific and decreased deep-water formation in the Southern Ocean. Data also indicate a switch from mostly thermally stratified to a salinity-stratified, isothermal deep ocean (Fig. 3).

4) Earliest Eocene (<55.25 Ma): The basinal $\delta^{13}C$ gradient was eliminated by 55.40 Ma, consistent with increased South Atlantic ventilation rates. $\delta^{13}C$ values begin to diverge by 55.28 Ma, coincident with the $\delta^{13}C$ recovery, with the highest ratios at the Atlantic and Southern Ocean sites and the lowest at the Pacific site. Bottom waters at the Pacific site were slightly warmer and fresher than at the Atlantic and Southern Ocean sites. As

such, an inferred decline in North Pacific overturning rates and increased deep-water formation in the Southern Ocean are associated with the $\delta^{13}C$ recovery.

These reconstructions support ocean modeling experiments representing Late Paleocene thermohaline circulation that predict convection in the Southern Hemisphere between Antarctica and Australia (*16*). Deep waters formed along the Antarctic margin would have filled the deep Pacific and Indian Ocean basins and mixed with intermediate waters in the Atlantic sector of the Southern Ocean to fill the deep South Atlantic basins. Magmatic activity and high heat flow associated with activity of the Iceland Plume is thought to have resulted in enhanced volcanic emissions of CO_2 and the emergence of a North Atlantic land bridge during the Latest Paleocene (*20*). These developments are modeled to have affected ocean circulation by driving an increase in North Pacific surface water salinities and a freshening of Southern Ocean surface waters. Rising CO_2 levels would be expected to have increased high-latitude precipitation, causing a decrease in Southern Ocean surface water salinities. The formation of the land bridge would have restricted the

flow of water from the Nordic Seas to the North Atlantic Ocean (*20*) and forced North Pacific surface water salinities to gradually rise, because of enhanced transport of saline thermocline waters from the subtropical North Atlantic into the North Pacific Basin through the Central American Seaway (*16*).

Downwelling in the North Pacific and deepened subtropical subduction during the Latest Paleocene would likely have caused warming of intermediate (Fig. 1) and thermocline (*7*) waters. This process could have destabilized regions of sedimentary methane hydrates and driven the $\delta^{13}C$ excursion (*4, 16*). The greatest amount of subduction-induced warming and carbon release is modeled to have occurred in Atlantic basins, consistent with the observation that Atlantic carbonate dissolution is much more pronounced than in the Pacific (*16*). Methane hydrate dissociation would have fueled initial PETM warming and hydrologic cycle changes, which in turn would have strengthened overturning rates in the North Pacific, weakened deep-water production in the Southern Ocean, and reduced ventilation rates in the South Atlantic. A threshold response to increasing surface water salinities near the Alaskan Margin
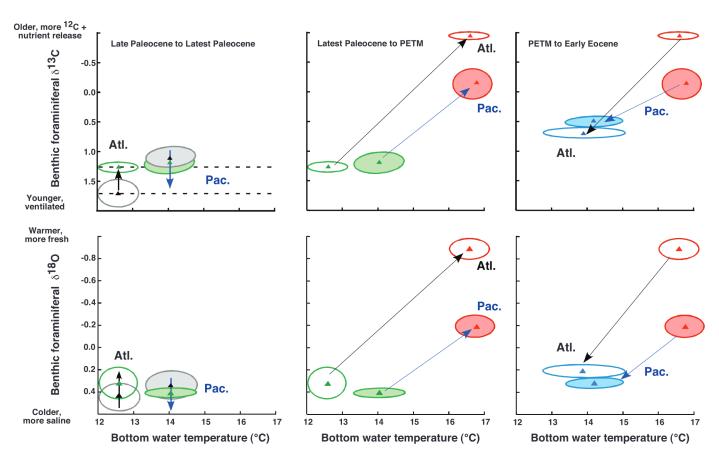

Fig. 4. Cross-plot for T_B versus benthic foraminiferal (top) $\delta^{13}C$ and (bottom) $\delta^{18}O$ across the PETM, illustrating the evolution of deep-water gradients between the North Pacific (Pac., shaded ellipses, Shatsky Rise site) and South Atlantic (Atl., open ellipses, Walvis Ridge site). Range (ellipses) and average values (triangles) are shown for specific time slices (gray, Late Paleocene; green, Latest Paleocene; red, PETM; and blue, Earliest Eocene). Dashed lines in the top left panel indicate Atlantic mean $\delta^{13}C$ values. Table S2 shows the change in slope of $\Delta\delta^{18}O/\Delta T_B$ before the PETM (between the Late Paleocene and the Latest Paleocene), indicating a change in the salinity contrast between the South Atlantic and North Pacific.

and salt contrast between the North Pacific and Southern Ocean would have been the sudden onset of deep convection in the North Pacific. Bottom waters formed would have filled deep Pacific basins and flowed through the Indonesian passage into the eastern Indian Ocean basin, and the locus of deep-water formation along Antarctica would have shoaled (16).

How would methane hydrate dissociation and an abrupt change in ocean circulation have affected climate? The injection of 2000 Gt of CH_4 into the oceans over ~10,000 years (the amount necessary to drive the $\delta^{13}C$ excursion) would have been insufficient to raise atmospheric CO_2 concentrations enough to drive whole-ocean warming of 4 to 5°C. The radiative forcing associated with a 70- to 160-ppmv increase in CO_2 would have caused only ~1°C warming (21), and therefore the clathrate hypothesis necessitates still unresolved climatic feedbacks to amplify and sustain PETM warmth.

The abrupt switch to convection in the North Pacific is modeled to have warmed the deep ocean by up to 3 to 5°C (Fig. 1) (16) and could have driven the PETM by maintaining high levels of atmospheric CO_2 and water vapor. Circulation-induced ocean warming could have driven additional increases in atmospheric CO_2 by destabilizing methane hydrates in deep ocean sediments (16). The solubility of CO_2 in seawater would also have decreased because of temperature and salinity changes, promoting higher atmospheric CO_2. Tropical ocean warming would have also promoted a more vigorous hydrologic cycle, higher evaporation rates, and saturation vapor pressures, resulting in increased levels of atmospheric water vapor (22), consistent with proxy data for surface water salinity (7, 8) and humidity (23, 24) across the PETM. The added radiative absorption from water vapor would have heightened the sensitivity of surface temperatures to rising atmospheric CO_2 and CH_4 concentrations, providing a strong positive feedback to warming (25, 26). The eventual sequestration of carbon through the biologic pump (17), terrestrial productivity (27), and weathering (28) would have resulted in global cooling over ~100,000 to 200,000 years. Associated temperature and hydrologic cycle changes would have driven a return to deep sinking in the Southern Hemisphere and shutdown of convection in the North Pacific (16).

References and Notes
1. J. P. Kennett, L. D. Stott, *Nature* **353**, 225 (1991).
2. E. Thomas, N. J. Shackleton, in *Correlation of the Early Paleogene in Northwest Europe*, R. W. O. Knox, R. M. Corfield, R. E. Dunay, Eds. (Geological Society Special Publication 101, London, 1996), pp. 401–441.
3. P. L. Koch, J. C. Zachos, P. D. Gingerich, *Nature* **358**, 319 (1992).
4. G. R. Dickens, J. R. O'Neil, D. C. Rea, R. M. Owen, *Paleoceanography* **10**, 965 (1995).
5. G. R. Dickens, M. M. Castillo, J. C. G. Walker, *Geology* **25**, 259 (1997).
6. G. A. Schmidt, D. T. Shindell, *Paleoceanography* **18**, 10.1029/2002PA000757 (2003).
7. A. Tripati, H. Elderfield, *Geochem. Geophys. Geosyst.* **5**, 10.1029/2003GC000631 (2004).
8. J. Zachos et al., *Science* **302**, 1551 (2003).
9. We analyzed *Oridorsalis umbonatus, Nuttallides truempyi,* and *Cibicidoides* spp. benthic taxa that have previously been used to reconstruct low-resolution T_B records for the Cenozoic and high-resolution records across the Eocene-Oligocene boundary (11). Seawater Mg/Ca can be considered constant over the duration of the PETM, because of the relatively long oceanic residence times of Ca (~10^6 years) and Mg (10^7 years) (29). The magnitude of warming calculated is therefore independent of seawater Mg/Ca ratio used. Absolute temperatures were calculated with current estimates for taxon-specific pre-exponential constants (30) and reconstructions of seawater Mg/Ca for 55 Ma (3.1 mmol/mol) (31).
10. Materials and methods are available as supporting material on *Science* Online.
11. C. Lear, H. Elderfield, P. Wilson, *Science* **287**, 269 (2000).
12. Shipboard Scientific Party, "Arctic Coring Expedition (ACEX): Paleoceanographic and tectonic evolution of the central Arctic Ocean" (Integrated Ocean Drilling Program Preliminary Report 302, ECORD, 2005), available at www.ecord.org/exp/acex/302PR.html.
13. D. K. Pak, K. G. Miller, *Paleoceanography* **7**, 405 (1992).
14. R. Corfield, J. Cartlidge, *Terra Nova* **4**, 443 (1992).
15. K. Miller, R. Fairbanks, G. Mountain, *Paleoceanography* **2**, 1 (1987).
16. K. L. Bice, J. Marotzke, *Paleoceanography* **17**, 9 (2002).
17. H. Stoll, S. Bains, *Paleoceanography* **18**, 10.1029/2002PA000875 (2003).
18. D. J. Thomas, T. J. Bralower, C. E. Jones, *Earth Planet. Sci. Lett.* **209**, 309 (2003).
19. D. J. Thomas, J. C. Zachos, T. J. Bralower, E. Thomas, S. Bohaty, *Geology* **30**, 1067 (2002).
20. R. W. Knox, in *Late Paleocene-Early Eocene Climatic and Biotic Events in the Marine and Terrestrial Record*, M. P. Aubry, S. G. Lucas, W. A. Berggren, Eds. (Columbia Univ. Press, New York, 1998), pp. 91–102.
21. H. Rennsen, C. J. Beefs, T. Fichefet, H. Goosse, D. Kroon, *Paleoceanography* **19**, 10.1029/2003PA000968 (2004).
22. A. Inamdar, V. Ramanathan, *J. Geophys. Res.* **103**, 32177 (1998).
23. C. Robert, J. P. Kennett, *Geology* **22**, 211 (1994).
24. G. J. Bowen, D. J. Beerling, P. L. Koch, J. C. Zachos, T. Quattlebaum, *Nature* **432**, 495 (2004).
25. S. Manabe, R. T. Wetherald, *J. Atmos. Sci.* **24**, 241 (1967).
26. D. Rind et al., *Nature* **349**, 500 (1991).
27. D. J. Beerling, *Palaeogeogr. Palaeoclimatol. Palaeoecol.* **161**, 395 (2000).
28. G. Ravizza, R. N. Norris, J. Blusztajn, M. P. Aubry, *Paleoceanography* **16**, 155 (2001).
29. W. S. Broecker, T. H. Peng, *Tracers in the Sea* (Eldigio, Palisades, NY, 1982).
30. C. Lear, Y. Rosenthal, N. Slowey, *Geochim. Cosmochim. Acta* **66**, 3375 (2002).
31. B. Wilkinson, T. Algeo, *Am. J. Sci.* **289**, 1158 (1989).
32. We thank W. Broecker for discussions; K. Bice, M. Bickle, S. Crowhurst, and A. Piotrowski for thoughtful reviews; R. Eagle for his support and advice; P. Rumford, B. Horan, and Gulf Coast Ocean Drilling Program Repository staff for provision of samples; and L. Booth, P. Ferretti, and M. Greaves for their invaluable technical help. This research used samples and data provided by the Ocean Drilling Program (ODP). Supported by the Comer Foundation.

Snowfall-Driven Growth in East Antarctic Ice Sheet Mitigates Recent Sea-Level Rise

Curt H. Davis,[1]* Yonghong Li,[1] Joseph R. McConnell,[2] Markus M. Frey,[3] Edward Hanna[4]

Satellite radar altimetry measurements indicate that the East Antarctic ice-sheet interior north of 81.6°S increased in mass by 45 ± 7 billion metric tons per year from 1992 to 2003. Comparisons with contemporaneous meteorological model snowfall estimates suggest that the gain in mass was associated with increased precipitation. A gain of this magnitude is enough to slow sea-level rise by 0.12 ± 0.02 millimeters per year.

Recent studies report substantial contributions from the Greenland (1, 2) and Antarctic (3, 4) ice sheets to present-day sea-level rise of ~1.8 mm/year (5). Rapid increases in near-coastal Greenland ice-sheet thinning (2) and West Antarctic glacial discharge (4) strengthen concern about accelerated sea-level rise caused by ice-sheet change. In contrast, the latest Intergovernmental Panel on Climate Change (IPCC) assessment predicts that overall, the Antarctic ice sheet will absorb mass during the 21st century due to increased precipitation in a warming global climate (6). Thus, increased precipitation over Antarctica could mitigate some of the mass loss from other terrestrial ice sources and their contributions to global sea-level rise. Here, we analyze elevation change of the Antarctic ice-sheet interior from 1992 to 2003 using nearly continuous satellite radar altimeter measurements. Because temporal variations in snowfall have been linked previously to decadal elevation change in Greenland's interior (7), we compare the observed elevation change to newly released meteorological model estimates of contemporaneous snowfall.